NeuroImage 100 (2014) 692–702

Contents lists available at ScienceDirect

NeuroImage

journal homepage: www.elsevier.com/locate/ynimg

The reorganization of corticomuscular coherence during a transition between sensorimotor states

Saeid Mehrkanoon [a,b,*], Michael Breakspear [a,b,d,e], Tjeerd W. Boonstra [a,b,c]

[a] School of Psychiatry, University of New South Wales, Sydney, Australia
[b] Black Dog Institute, Sydney, Australia
[c] MOVE Research Institute, VU University, Amsterdam, The Netherlands
[d] QIMR Berghofer Medical Research Institute, Brisbane, Australia
[e] Royal Brisbane and Women's Hospital, Brisbane, Australia

ARTICLE INFO

Article history:
Accepted 22 June 2014
Available online 30 June 2014

Keywords:
Motor control
Corticomuscular coherence
Dual-band synchronization
Prediction errors

ABSTRACT

Recent research suggests that neural oscillations in different frequency bands support distinct and sometimes parallel processing streams in neural circuits. Studies of the neural dynamics of human motor control have primarily focused on oscillations in the beta band (15–30 Hz). During sustained muscle contractions, corticomuscular coherence is mainly present in the beta band, while coherence in the alpha (8–12 Hz) and gamma (30–80 Hz) bands has not been consistently found. Here we test the hypothesis that the frequency of corticomuscular coherence changes during transitions between sensorimotor states. Corticomuscular coherence was investigated in twelve participants making rapid transitions in force output between two targets. Corticomuscular coherence was present in the beta band during sustained contractions but vanished before movement onset, being replaced by transient synchronization in the alpha and gamma bands during dynamic force output. Analysis of the phase spectra suggested a time delay from muscle to cortex for alpha-band coherence, by contrast to a time delay from cortex to muscle for gamma-band coherence, indicating afferent and efferent corticospinal interactions respectively. Moreover, alpha and gamma-band coherence revealed distinct spatial topologies, suggesting different generative mechanisms. Coherence in the alpha and gamma bands was almost exclusively confined to trials showing a movement overshoot, suggesting a functional role related to error correction. We interpret the dual-band synchronization in the alpha and gamma bands as parallel streams of corticospinal processing involved in parsing prediction errors and generating new motor predictions.

Introduction

Synchronous brain rhythms represent a dynamic mechanism for coordinating neural activity across large-scale neuronal networks and controlling the timing of neuronal firing (Buzsaki and Draguhn, 2004; Engel et al., 2001; Wang, 2010). Evidence from the past two decades of research suggests that neural oscillations subserve important cognitive functions, including motor control (Fetz, 2013; Fries, 2005; Schnitzler and Gross, 2005). During sustained contractions, primary motor cortex shows oscillations in alpha (8–12 Hz) and beta (15–30 Hz) bands (Baker et al., 2003; Murthy and Fetz, 1992; Sanes and Donoghue, 1993). Although oscillations in both frequency bands are effectively carried down the corticospinal tract (Baker et al., 2003), most studies using sustained contractions find that only beta-band oscillations are coherent between motor cortex and muscle activity (Baker et al., 1997; Conway et al., 1995; Gross et al., 2000; Halliday et al., 1998). Corticomuscular beta-band coherence is most prominent during tonic muscle contractions and disappears during movement (Baker et al., 1997, 1999; Kilner et al., 2000; Riddle and Baker, 2006) and beta-band activity is enhanced when higher precision is required (Gilbertson et al., 2005; Kristeva et al., 2007; Kristeva-Feige et al., 2002; Witte et al., 2007). These findings suggest that the beta-band activity is related to a mechanism that maintains the current sensorimotor state (Baker, 2007; Engel and Fries, 2010; Van Wijk et al., 2012).

Research findings of corticomuscular coherence at other frequencies are inconclusive. A few studies have reported alpha-band coherence during sustained contractions (Raethjen et al., 2002) and during slow finger movements (Gross et al., 2002; Williams et al., 2009). It has recently been proposed that a spinal circuit may reduce 10-Hz oscillations in descending cortical input to the spinal motor neurons (Williams et al., 2010). In particular, computational analyses have shown that recurrent inhibition via Renshaw cells in the spinal cord leads to partial cancellation of 10 Hz oscillations, markedly reducing corticomuscular coherence at this frequency (Williams and Baker, 2009). Corticomuscular gamma-band coherence has been observed during dynamic force output (Cheyne et al., 2008; Omlor et al., 2007), as well as during movement

* Corresponding author at: Black Dog Institute, Hospital Rd, Randwick, NSW 2031, Australia.
E-mail address: smehrkanoon@gmail.com (S. Mehrkanoon).

http://dx.doi.org/10.1016/j.neuroimage.2014.06.050
1053-8119/

preparation (Schoffelen et al., 2005, 2011). These results indicate that the frequency of corticomuscular coherence varies across motor tasks and may hence be dependent on the moment-to-moment motor state (Marsden et al., 2000).

An overarching framework suggests that different carrier frequencies reflect different types of neural processing, predicting changes in the frequency of corticomuscular coherence during transitions in sensorimotor state, e.g. from sustained contractions to dynamic force output (Engel and Fries, 2010). Here we test this hypothesis by investigating corticomuscular coherence while participants make fast transitions between two distinct force levels. We hypothesized that corticomuscular coherence in the beta band would disappear during dynamic motor output and that coherence at other frequencies would appear during the transition between force levels. Phase spectra are used to characterize the type of interaction underlying the observed functional connectivity. Capturing the reorganization of the dynamics in the sensorimotor loop speaks to the functional role of corticomuscular coherence and its role in coordinating the information transfer between sensorimotor cortex and spinal populations.

Materials and methods

Participants

Twelve healthy right-handed adults (age: 28.5 ± 2.7 years; 8 males and 4 females) participated as paid volunteers in this study. The protocol was approved by the Human Research Ethics Committee of The University of New South Wales. All participants gave voluntary and informed consent according to National Health and Medical Research Council guidelines.

Experimental design

The experiment involves a sensorimotor loop (Wolpert and Ghahramani, 2000): Vibrotactile stimuli were delivered to the same index finger used for force generation. This setup was chosen to approximate a closed loop system, which requires minimal interactions with other brain systems. By using vibrotactile stimuli with linearly increasing amplitude the study seeks to investigate the reorganization of corticomuscular dynamics inherent to the sensorimotor loop and not those imposed through sudden, large amplitude perturbations. Participants were seated in a light- and sound-attenuated room with their right hand on a flat panel and their forearm supported. They were instructed to generate isometric force by abducting their index finger against a force sensor (Fig. 1C). Participants received visual feedback of the exerted force and were instructed to keep their force output within predefined force intervals (target 1: 0.5–0.9 N, target 2: 1.1–1.5 N) displayed on the computer screen (Fig. 1A). Both force targets were visible throughout the trial and participants had to make a transition between force targets upon perceiving the vibrotactile 'go' cue. Participants were instructed to move the cursor within target 1 at the start of each trial and keep it there until they perceived a vibration delivered to their index finger. After a variable time interval (4–7 s), a vibrotactile stimulus was delivered to the index finger that generates the force output. The amplitude of the stimulus linearly increased from zero (Fig. 1D) and once participants perceived the vibration, they had to move the cursor into target 2 as quickly as possible and keep it within target 2 until the end of the trial. The vibration was ceased immediately when a movement was performed.

Vibrotactile stimuli consisted of pure sinusoidal vibrations at a single frequency that were delivered to the index finger by a shaker attached to the force sensor. The amplitude of the stimuli increased linearly over a 8-s time interval. This slowly ramped increase was employed to avoid sensory evoked cortical activity associated with sudden suprathreshold stimuli. Each condition was repeated in 16 trials and each participant received 80 trials in total (16 trials × 5 stimulus frequencies). The stimulus frequency was varied across five stimulus conditions (14, 18, 22, 26, and 30 Hz). Prior to the experiment, the amplitude of the vibrotactile stimulus for each subject was titrated to the individual perception threshold such that the final amplitude of the stimulus (at 8 s) was equal to 3× threshold (Fig. 1D).

Data acquisition

A force sensor (LSB200 L2357, JR S-Beam load cell, FUTEK, California, USA) was used to measure the force exerted by the participant. The load cell was mounted onto a small mechanical shaker (Gearing and Watson Electronics, Hailsham, East Sussex, UK) that delivered the vibrotactile stimuli to the index finger. Participants were instructed to exert isometric force against the load cell by abducting their index finger. The locations of the thumb and fingers were fixed to ensure a 60° angle between thumb and index finger and avoid the generation of force by the other fingers by co-contraction of synergist hand muscles (Fig. 1C). The force signal was amplified (SCG110, Strain Gage Amplifier, FUTEK, California, USA) and digitized at 1 kHz (NI USB-6259 BNC, National Instruments, Austin, Texas).

Surface EEG and EMG were acquired using a 64-channel amplifier — BrainAmp MR Plus (Brain Products, Munich, Germany) and custom electrode caps (Easy Cap, Falk Minow Services, Herrsching-Breitbrunn, Germany, Fig. 1B). EEG electrodes were arranged according to the international 10–20 system. Two channels were used for the electrocardiogram, one for the electrooculogram, and two for EMG, leaving 59 scalp EEG channels. All data were referenced against an electrode centered on the midline between Fz and Cz and impedances at all electrodes were kept below 5 kΩ. EEG data were band-pass filtered (0.5–80 Hz). An independent component analysis (ICA) algorithm, InfoMax (Cardoso, 1997), was used to identify and remove cardiac, ocular and muscular artifacts. EEG data were re-referenced to the average reference. A bipolar derivative was taken from the EMG electrodes and the resulting EMG signal was full-wave rectified using the Hilbert transform, which is optimal for assessing corticomuscular coherence at low force levels (Boonstra and Breakspear, 2012; Farina et al., 2013; Ward et al., 2013). The resulting EEG and EMG signals were then downsampled to 1 kHz.

Data analysis

To capture the changes in corticospinal synchronization during the execution of the transition between the two force levels, time–frequency coherence was estimated pair-wise between all EEG channels and the rectified EMG signal. Time-resolved coherence quantifies linear correlations between two observables $x[n]$ and $y[n]$, as a function of time and frequency. Let $x[n]$ and $y[n]$ be a single EEG and rectified surface EMG signal respectively. As in Mehrkanoon et al. (2013), we define the complex-valued time–frequency coherency function as

$$\hat{\Gamma}_{xy}[t,f] = \frac{S\left\{\hat{p}_{xy}[t,f]\right\}}{\sqrt{S\{\hat{p}_{xx}[t,f]\}S\left\{\hat{p}_{yy}[t,f]\right\}}}\, t = 1,2,\ldots,N, \tag{1}$$

where $\hat{p}_{xy}[t,f]$ denotes the Fourier cross-spectral density (CSD) estimate between signals $x[n]$ and $y[n]$, and $\hat{p}_{xx}[t,f]$ denotes the power spectral density (PSD) estimate. Fourier based spectral decomposition was performed by using a unit power Hamming window of 0.75-s duration. The smoothing operator $S\{.\}$ used in this analysis is given by

$$K(n,k) = \exp\left(-\left(\frac{n^2}{2\sigma_n^2} + \frac{k^2}{2\sigma_k^2}\right)\right), \tag{2}$$

where $\sigma_n = 0.66$ s and $\sigma_k = 1.32$ Hz denote the time and frequency spreads of the Gaussian kernel. Smoothing was implemented by

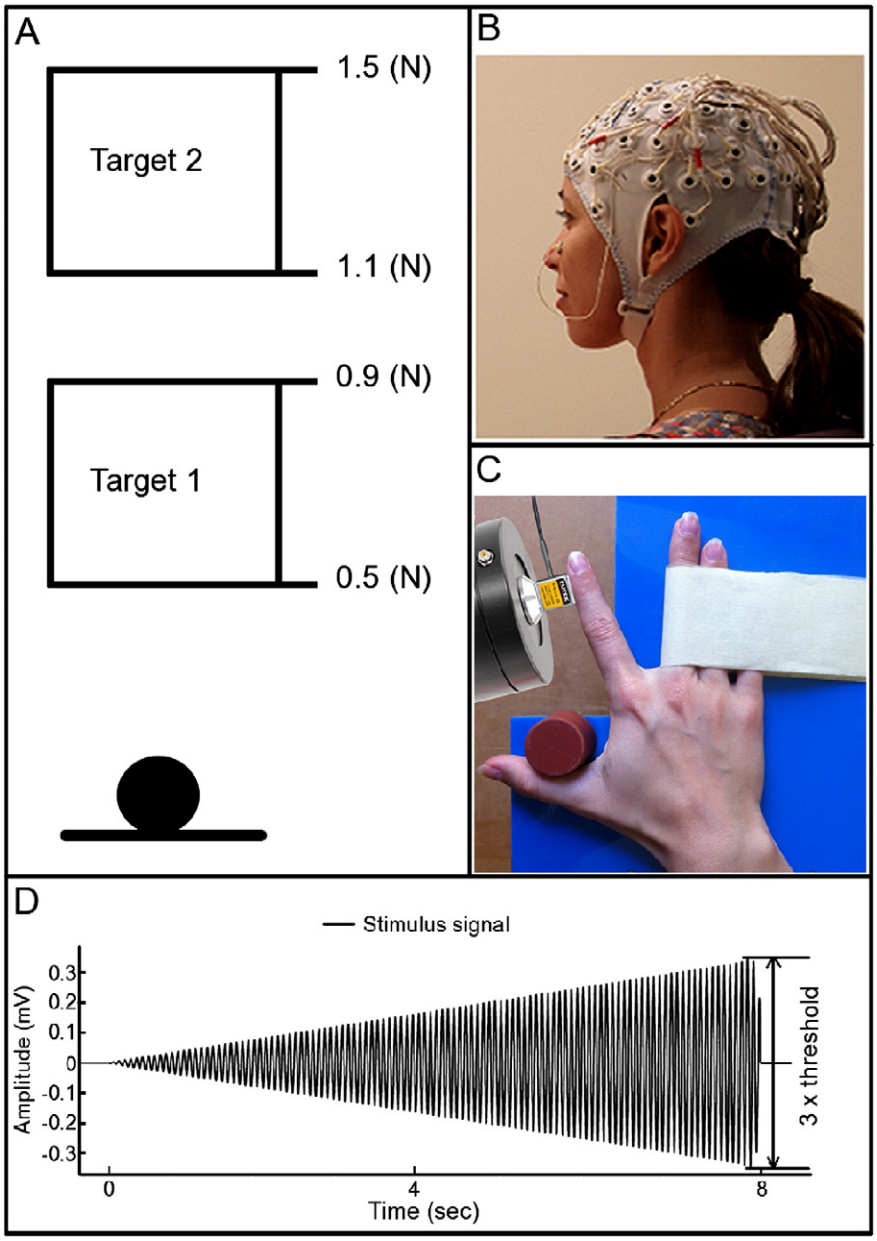

Fig. 1. Task design. (A) Diagram of visual feedback showing the two force targets. (B) Participant with an EEG cap. (C) Diagram of experiment setup. Subject exerted isometric force by abducting their index finger against a force sensor. The force sensor was mounted on a mechanical shaker that delivered vibrotactile stimuli to the index finger. (D) Example of vibrotactile stimulus. The amplitude of a sinusoid linearly increased over a time interval of 8 s to 3× the perceptual threshold.

convolving the kernel $K(n,k)$ with the time–frequency coherency to improve the reliability of the coherency estimate (Mehrkanoon et al., 2013).

Two markers indicating the start and endpoint of movement were identified for the purpose of data alignment across trials. The moving average and standard deviation were first calculated across all trials. The movement start point was then defined as the time point at which the generated force crossed above one standard deviation of the moving average. The maximum force production within the 2 s time interval after the start point was used to identify the endpoint of movement. This calculation was performed for every trial. Trials were aligned with respect to the endpoint of movement. Note that herein we refer to the movement endpoint as $t = 0$. Time–frequency coherency estimated in each trial was aligned with respect to the endpoint of movement and the complex-valued coherency was averaged across 80 trials to further improve the signal-to-noise ratio of the estimate. We study the motor response irrespective of the frequency of the vibrotactile stimuli, hence collapsing the analysis across the five stimulus conditions. After averaging, the magnitude-squared coherence was obtained. Averaging complex valued coherency across trials is equivalent to the 'pooled coherence' procedure described in Amjad et al. (1997). In addition to the coherence spectra, the Fourier-based power spectra of EEG channels C3 and CP3 and the rectified EMG were estimated. We converted the individual power spectra of EEG and EMG to percentage change. To this end, the mean value of the power spectrum was calculated at each frequency for the time interval of −8 to 4 s. The mean was then subtracted from the power spectra at each frequency and then divided by the mean to render a percentage change from the average.

In addition to the magnitude-squared coherence, we also investigated the phase difference captured by the phase spectra of the complex-valued coherency estimate. The phase spectra contain information on the temporal relation between EEG and EMG (Mima et al., 2000). A delay in the time domain corresponds to a phase offset in the frequency

domain (Stam et al., 2007). The phase offset and time lag were determined from the phase spectra. A constant time lag between two signals results in a linear trend in the phase difference across frequencies, which has indeed been observed for corticomuscular coherence (Raethjen et al., 2002; Riddle and Baker, 2005; Schoffelen et al., 2005). The slope of the phase spectrum can be estimated by fitting a line to the phase spectrum across a frequency range of interest, which provides a reliable measure of the time lag (Halliday et al., 1995; Mima et al., 2000). We used a weighted linear regression model to estimate the slope and phase offset of the phase spectra. The phase difference at a specific frequency, f, between signals $x[n]$ and $y[n]$ is given by

$$\theta_{xy}(f) = 2\pi f\tau + \theta_0 = mf + \theta_0, \tag{3}$$

where τ denotes the delay, θ_0 is the phase offset or the constant phase shift, and m is the slope of the phase difference (Mima et al., 2000). The time lag (in ms) was directly calculated from the estimated slope as

$$\tau = \frac{m}{2\pi} \times 1000[\text{ms}]. \tag{4}$$

Hence the recorded phase difference θ_{xy} is determined by the phase offset and the time lag and both were used to characterize the interactions between EEG and EMG.

Statistical analysis

We used a two-stage summary statistics approach, i.e. a mixed effects model, to apply family-wise correction to the significance threshold of time–frequency coherence (Friston et al., 1995; Poline et al., 1997; Worsley and Friston, 1995). First, we converted magnitude-squared coherence of individual participants to z-scores. Subsequently, we converted the individual z-scores into a group-level t-value. Both z-scores and t-values were defined for each time–frequency point and hence involve multiple comparisons. The 2D Gaussian smoothing kernel used to compute time–frequency coherence introduces correlations between neighboring time–frequency points. Random field theory was then used to correct for multiple comparisons exploiting the known correlation structure (Siegmund and Worsley, 1995; Worsley, 2001). Since this is the first application of random field theory to time–frequency coherence analysis, we describe this procedure in further detail below.

Z-statistic for single subject data

The null distribution of the time–frequency coherence estimates was first constructed by randomizing the Fourier phases of the time–frequency coherence estimates before averaging across 80 trials. 1000 realizations were performed to construct the null distribution by using the Fourier phase randomization approach (Kants and Schreiber, 2003). This null represents the distribution of coherence in the case where there is no systematic relationship between EEG and EMG. The z-score can then be defined for the ith participant as follows,

$$Z_i(t,f) = \frac{|\hat{\gamma}_i(t,f)| - |\mu_i(t,f)|}{\sigma_i(t,f)}, \tag{5}$$

where $|\hat{\gamma}(t,f)|$ denotes the absolute value of the averaged time–frequency coherence estimates over the channels and trials, $|\mu_i(t,f)|$ is the absolute value of the surrogate estimate, and $\sigma_i(t,f)$ is the standard deviation of the constructed surrogate data.

T-statistic across participants

To calculate the t-statistic across participants the z-scores of each of the 12 participants were considered as new variables in a second-level analysis. Let $\mathbf{Z}(t,f) = [Z_1(t,f), \ldots, Z_{12}(t,f)]$ such that $\mathbf{Z}(t,f) \in \mathbb{R}^{(t \times f \times 12)}$ be a data array where its entries are the z-scores given in Eq. (5) for each subject. The hypothesis $H_0 : \mathbb{E}[Z_i(t,f)] = 0$ assumes that the entries of the z-scores $\mathbf{Z}(t,f)$ are normally distributed (i.e., $Z_i(t,f) \sim \mathcal{N}(0, \sigma_{z_i})$). To examine whether the hypothesis H_0 is rejected or not, a one-sample t-test was performed in order to compare the z-scores across the 12 participants against zero,

$$\underset{\text{group}}{T}(t,f) = \frac{\underset{\text{subject}}{\mathbb{E}}[\mathbf{Z}(t,f)]}{\sigma_z(t,f)/\sqrt{12}}, \tag{6}$$

where $\underset{\text{group}}{\mathbb{E}}[\mathbf{Z}(t,f)]$ and $\sigma_z(t,f)$ denote the average and standard deviation of the z-scores array $\mathbf{Z}(t,f)$ across participants. The group-level significance value at $p < 0.05$ was then calculated by using an approach, family-wise error correction (Poline et al., 1997), to correct for the multiple comparisons.

Random field theory

Several approaches including parametric and non-parametric techniques obtained from random field theory (RFT) have recently been proposed to correct for the multiple comparisons in fMRI research (Friston et al., 1995; Worsley and Friston, 1995). Using RFT yields a conservative estimate for the family-wise error rate (FWER) using the combined spatial extent and peak intensity (Poline et al., 1997; Worsley et al., 1992). One of the most common approaches in RFT used to correct the p-value is based on the Euler characteristic (EC) that has been adapted to volume-extent statistics, namely the cluster-wise approach (Worsley et al., 1992). The EC reformulates the geometric problem as a topological problem by thresholding the voxels, and thus accounts for the number of connected voxel clusters remaining in the field of interest. It has been previously shown that the expected EC, $\mathbb{E}[\text{EC}]$, approximately corresponds to the probability of FWER. The expected EC of the z-statistic can then be defined as follows:

$$\mathbb{E}[\text{EC}] = R(4\log_e 2)^{\frac{3}{2}}(2\pi)^{-2}\left(Z^2-1\right)\exp\left(-\frac{Z^2}{2}\right), \tag{7}$$

where $\mathbb{E}$ denotes the mathematical expectation, R denotes the number of Resels (or resolution of elements, the ratio of the smoothing kernel's volume to the brain volume, or here the ratio of the smoothing kernel's area to the area of the time–frequency plane), and Z is the z-score thresholds. The set of z-score thresholds and their expected value derived from equation Eq. (7) corresponds to the probability of a family-wise error (Poline et al., 1997; Worsley et al., 1992). Hence, we adopt this approach commonly used in fMRI analysis for the analysis of significant time–frequency points, by exploiting the known correlation structure induced by the 2D Gaussian smoothing kernel used in estimation of time–frequency coherence.

Phase analysis

At those frequencies where the coherence remained significant after FWE correction, we then used the phase spectra to estimate the corticomuscular phase offset and time lag for these frequencies. For this phase analysis we used data from those participants for which coherence in these frequency ranges exceeded the within-subject significance threshold. Comparison across the resulting significant frequency bands was conducted using an unpaired two-sample t-test for nonequivalent sample sizes. Circular statistics were used for comparing the phase offsets.

Results

Participants were instructed to keep their force output within the first target (0.5–0.9 N) until they perceived a slowly increasing vibrotactile stimulus delivered to their index finger. Once they perceived a vibration, they had to change their force output as quickly as possible and keep it within target 2 (1.1–1.5 N) until the end of each trial. Fig. 2A shows the average force signal across trials and participants. Steady-state motor output can be observed in the time intervals of −8

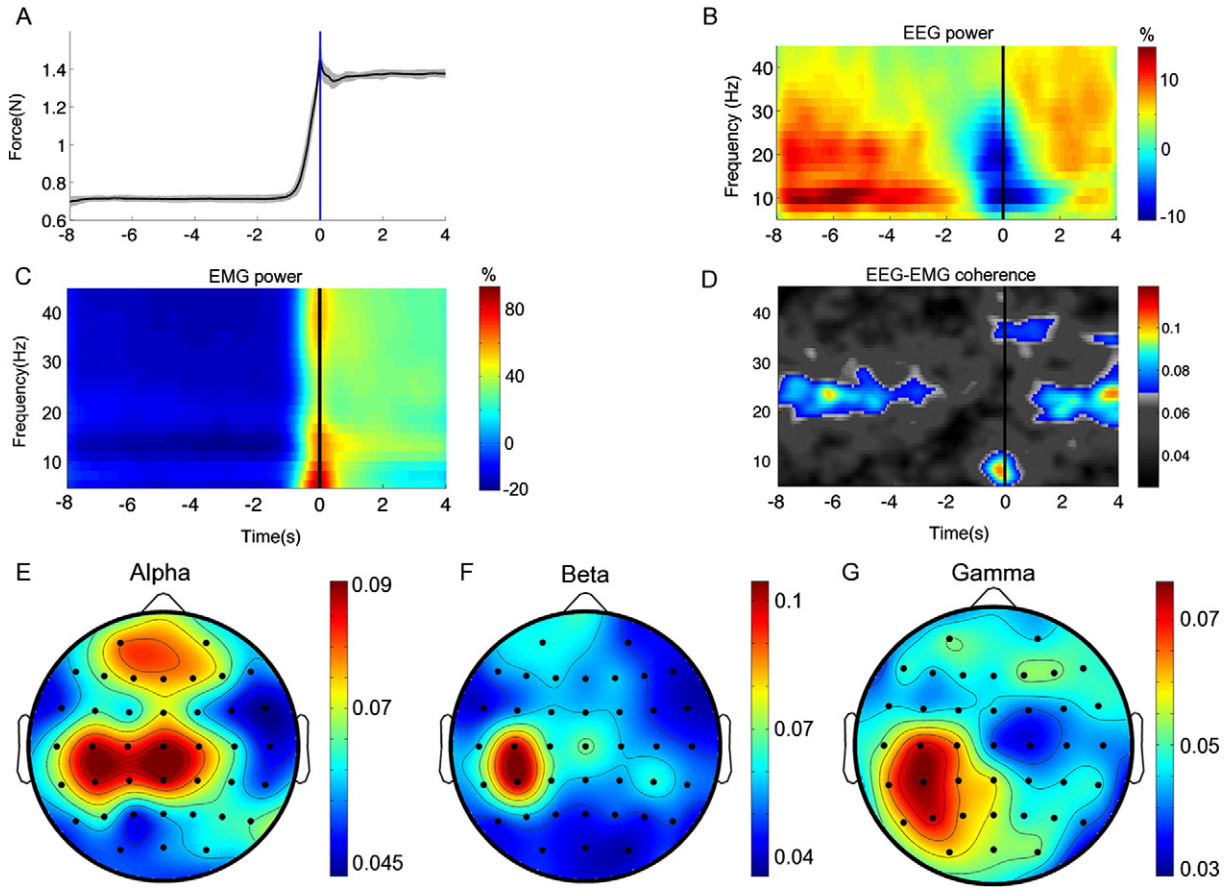

Fig. 2. Grand-average force profiles and time–frequency spectra. (A) Force profile, where $t = 0$ corresponds to the endpoint of movement. Gray patch reveals the across-participants standard deviation of the force profile. (B) Power spectra of EEG acquired from channels C3 and CP3 showing the percent change from the average. (C) Power spectra of rectified EMG showing the percent change from the average. (D) Magnitude-squared coherence of EEG and rectified EMG. Suprathreshold coherence ($p < 0.05$, FWE corrected) is represented by color. Panels E–G show the spatial topology of corticomuscular coherence in (E) the alpha band (9 Hz at $t = 0$), (F) the beta band (22 Hz, from −7 to −4 s) and (G) the gamma band (37.5 Hz at $t = 0$).

to −1 s and 1 to 4 s, while dynamic motor output is observed on the interval of −1 to 1 s. The average time delay between the onset of the vibrotactile stimuli and the onset of movement was 3.87 ± 1.48 s (mean ± sd). The average duration of the transition from target 1 to target 2 was 0.82 ± 0.056 s. The average peak force at the end of movement (i.e., at $t = 0$) was 1.45 ± 0.05 N.

Figs. 2B and C show the corresponding power spectra of EEG signals (recorded from channel C3 and CP3) and the rectified EMG respectively. A marked reduction in EEG power in the alpha and beta bands appears during the transition from target 1 to target 2, i.e. during the time interval of −1 to 1 s. By contrast, the transition to the higher force level is accompanied by an increase in power of rectified EMG along all frequencies (Fig. 2C), particularly in the alpha and gamma bands. A small reduction in EMG power can be observed once the force output is stabilized within the second target range.

Statistically significant coherence ($p < 0.05$, FWE corrected) in the beta band (~20–25 Hz) appears during steady state motor output — that is, when participants kept their force constant within one of the force targets (Fig. 2D). Beta-band coherence was reduced well before the onset of the transition between force targets and completely absent during dynamic force output. While coherence in the beta band was absent, significant coherence was observed in the alpha band (5–12 Hz, maximum at 9 Hz) around the movement endpoint ($t = 0$). In addition, significant corticomuscular gamma-band (34–40 Hz) coherence appears in the time interval of −0.5 to 2 s. When the force output was stabilized in the second force target, beta-band coherence reappeared approximately 2 s after the movement endpoint. The frequency of the vibrotactile stimulus was 14, 18, 22, 26 or 30 Hz. The preceding results were obtained by pooling data across all trials, and hence across all of these stimuli. To investigate the potential effect of specific stimulus frequencies on the strength of corticomuscular coherence, we computed corticomuscular coherence separately for each stimulus frequency and re-analyzed those effects that were significant in the grand averages i.e. the beta band during static motor output and the alpha and gamma bands during dynamic motor output. A repeated-measures ANOVA showed that there were no systematic effects of stimulus frequency on corticomuscular coherence in these three frequency bands ($p > 0.1$ see Supplementary material).

The spatial topologies of corticomuscular coherence for these three distinct frequency regimes are shown in Figs. 2E–G. Although all three topologies reveal maximal corticomuscular coherence in channels over the contralateral sensorimotor area, there are clear differences in their spatial distributions: Beta-band coherence showed a single maximum over channel C3 and CP3, whereas corticomuscular coherence in the alpha band revealed a more distributed pattern with multiple maxima. In addition to the maxima over channels C3 and CP3, two maxima were observed over the central midline at channels Cz–CPz and at channels Fz–FPz respectively. The topology of gamma-band coherence again showed a single maximum over C3–CP3 similar to beta-band coherence, although coherence was generally weaker and more spatially diffuse.

The grand-average coherence and phase spectra during steady-state motor output (−7 to −4 s) and dynamic force output (−0.5 to 0.5 s) are presented in Fig. 3. During steady-state motor output, significant corticomuscular coherence was present in the frequency range of 18 to 27 Hz (Fig. 3A). The corresponding phase spectrum (Fig. 3B) shows

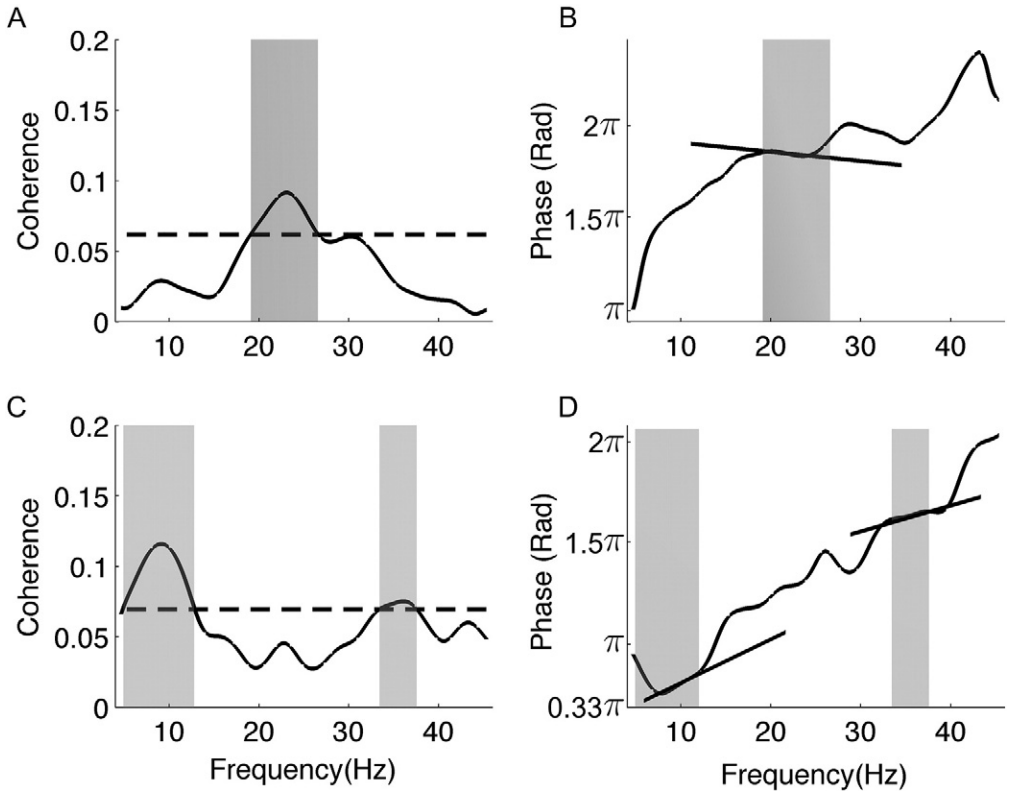

Fig. 3. Grand-average coherence and phase spectra. (A) Magnitude-squared corticomuscular coherence on the interval of −7 to −4 s. Significant coherence indicated by gray patches ($p < 0.05$). (B) Corresponding phase spectra and fitted regression line in the beta band. (C) Magnitude-squared coherence at interval −0.5 to 0.5 s showing significant coherence in the alpha and gamma frequency bands. (D) Corresponding phase spectra with regression lines in the alpha and gamma bands.

that the phase difference in this frequency range is ~2π. The phase slope estimated using weighted linear regression revealed a negative slope of −0.015 rad/Hz corresponding to a time delay from EEG to EMG of 2.4 ms. By contrast, corticomuscular coherence in the time interval of −0.5 to 0.5 s was statistically significant in the frequency range of 5–12 Hz (Fig. 3C) – where coherence was maximal at 9 Hz – with a phase difference close to 0.5π (Fig. 3D). The slope was positive (0.051 rad/Hz) corresponding to a time lag from EMG to EEG of 8.1 ms. During this time interval, significant coherence was also present in the gamma range (33–39 Hz) with a phase difference close to 1.5π. The slope was positive (0.032 rad/Hz) corresponding to a time lag from EMG to EEG of 5.1 ms.

To statistically compare the phase offset and slope for the three frequency regimes, we repeated the same analysis for the coherence and phase spectra of individual participants. Because the phase can only be reliably estimated when there is statistically significant coherence, we only used those participants showing significant corticomuscular coherence in the alpha (8–12 Hz), beta (15–30 Hz), and gamma (30–45 Hz) frequency bands. Table 1 lists the results for all 12 participants. In the alpha and gamma frequency ranges (obtained from the time interval of −0.5 to 0.5 s), 7 of the 12 participants showed corticomuscular coherence that exceeded the 95% confidence interval. Using a weighted linear regression approach, the average phase offset θ_0 was 2.6 and the slope −0.032 rad/Hz for alpha frequency band. This slope corresponds to a 5.2 ms time lead of the EMG signal. In the beta band, 8 of the 12 participants showed significant coherence and the average phase offset was 5.6 rad and the slope 0.069 rad/Hz corresponding to a 11.0 ms time lag. For the gamma band, the phase offset across 7 participants was 5.2 rad and the slope 0.069 rad/Hz corresponding to 11.1 ms time lag of the EMG signal.

Table 1
Phase relationship of significant corticomuscular coherence in the alpha, beta, and gamma bands.

Subject	Alpha				Beta				Gamma			
	Freq	θ_0	Slope	Time-lag	Freq	θ_0	Slope	Time-lag	Freq	θ_0	Slope	Time-lag
1	4–12	2.4	0.053	8.4	18–23	−0.8	0.08	13.4	33–40	−0.38	0.09	14.9
2	–	–	–	–	17–27	6.3	−0.001	−0.2	31–40	−1.7	0.12	19.5
3	–	–	–	–	28–29	−0.7	0.07	10.5	37–40	4.5	−0.18	−28.6
4	4–11	3.9	−0.12	−19.1	14–24	2.8	0.15	23.2	30–40	−1.0	0.12	19.1
5	–	–	–	–	18–27	4.8	0.01	2.2	–	–	–	–
6	7–8	1.3	−0.03	−4.8	–	–	–	–	–	–	–	–
7	5–12	3.9	−0.10	−15.9	–	–	–	–	35–38	−1.5	0.12	19.5
8	6–8	3.5	−0.20	−31.8	–	–	–	–	–	–	–	–
9	5–12	1.2	0.14	22.3	24–28	1.0	0.16	25.5	–	–	–	–
10	–	–	–	–	19–26	6.0	−0.02	−3.8	37–40	−0.94	0.13	20.7
11	6–12	2.0	0.03	4.8	–	–	–	–	–	–	–	–
12	–	–	–	–	21–28	3.2	0.11	17.5	34.5–38.5	−0.06	0.08	12.7

Freq: Frequency range (in Hz) showing significant corticomuscular coherence ($p < 0.05$); θ_0: the constant phase offset (in rad) determined using linear regression analysis of phase spectra (Eq. (3)); slope (in rad/Hz): the linear trend of the regression analysis; τ: the time lag (in ms) between EEG and EMG obtained from the slope m (Eq. (4)).

Because different participants showed significant coherence in the alpha, beta and gamma bands, we used an unpaired two-sample t-test to compare the phase offset and time lags across frequency bands. The phase offset ($t(15) = 1.87$, $p = 0.04$) and the time lag ($t(15) = 2.1$, $p = 0.026$) were significantly different between the alpha and beta band. The phase offset and time lags in alpha band were also significantly different from the phase offset in gamma band ($t(14) = 2.67$, $p = 0.009$) and ($t(14) = 1.72$, $p = 0.053$) respectively. Finally, the phase offset in beta band was not significantly different from the phase offset in gamma band ($t(14) = 0.77$, $p = 0.22$). The time lags in beta and gamma bands were also not significantly different ($t(14) = 0.19$, $p = 0.42$).

The grand-average coherence spectra hence revealed a clear change in the frequency content of corticomuscular coherence during the transition from steady state to dynamic motor output, as well as the phase relationship between EEG and EMG. To further explore corticomuscular coherence in the alpha and gamma range during the transition between force levels, we partitioned the trials into three different subgroups based on their force profiles. In particular, we sorted the 80 trials in each subject based on the maximum force level at $t = 0$: Trials in subgroup 1 consisted of those 26 trials in each subject with the greatest maximum force; subgroup 2 consisted of the middle 26 trials; and subgroup 3 the lowest 26 trials. We then averaged the complex-valued time–frequency coherence across 26 trials for each subgroup separately and analyzed magnitude-squared coherence identically to the original analyses. The maximum force at $t = 0$ for 3 subgroups was 1.62 ± 0.20 N, 1.46 ± 0.12 N, and 1.30 ± 0.09 N respectively. As expected, the maximum force for subgroup 1 was significantly higher than the force in subgroup 3 ($t(12) = 3.2$, $p = 0.003$). The movement duration, i.e. the time between the onset and offset of the movement, was 0.71 ± 0.05 s, 0.85 ± 0.06 s, and 0.92 ± 0.05 s for subgroups 1 to 3 respectively, and was significantly shorter in subgroup 1 than for subgroup 3 ($t(12) = 2.85$, $p = 0.007$). The average reaction time, i.e. the time delay between the onset of the vibrotactile stimuli and the onset of movement, was 3.61 ± 0.14 s for subgroup 1 and 4.1 ± 0.24 s for subgroup 3, and was significantly shorter in subgroup 1 than for subgroup 3 ($t(12) = 2.18$, $p = 0.024$).

The force profile and corticomuscular coherence spectra in the three subgroups are shown in Fig. 4. As expected, the force profiles of the first subgroup show a higher maximum force at the movement endpoint compared to subgroups 2 and 3. An overshoot to 1.6 N is visible in the first subgroup that is followed by a correction back to the center of the second force level (1.3 N). The overshoot is attenuated in the second subgroup (1.46 N) and absent in the last subgroup. Note that no undershoot was observed in subgroup 3. Comparing the coherence spectra of the three subgroups (Fig. 4B) reveals a pronounced increase in corticomuscular coherence in the alpha and gamma bands around the movement endpoint (i.e., $t = 0$) in trials showing the largest overshoot (subgroup 1). While alpha-band coherence around the movement endpoint is still visible in the second subgroup, it is much reduced compared to subgroup 1. In addition, gamma-band coherence is largely absent. Finally, in the last trial subgroup – showing no overshoot – corticomuscular coherence at $t = 0$ is largely absent across frequencies.

To statistically test the reduction of corticomuscular coherence, we derived the z-score of subgroup 1 versus subgroup 3 trials (Fig. 5), confirming significantly higher coherence in the alpha and gamma bands at $t = 0$. The spatial topology of the z-scores for the alpha band (Fig. 5B) and the gamma band (Fig. 5C) is largely similar to the topologies for the grand-average results (Figs. 2E, G). Together these analyses show that corticomuscular coherence in the alpha and gamma bands are largely driven by the trials in which the participants make the largest overshoot in force production, followed by correction back to the center of target 2.

Discussion

To investigate the changes in carrier frequencies during a transition in sensorimotor state, we examined corticomuscular time–frequency coherence during fast transitions between two force targets. Consistent with previous studies we found significant coherence in the beta band during constant force output that diminished well before movement onset and was completely absent during the transition to the second force target. During dynamic force output, beta-band coherence was replaced by coherence in the alpha and gamma bands, which were both maximal at the endpoint of movement. Beta-band coherence reappeared following the stabilization of force output in the second target. Coherence in the alpha and gamma bands was most strongly expressed in trials that showed the fastest transition between targets and which were accompanied by an overshoot when reaching the second target. Corticomuscular coherence in the beta and gamma bands

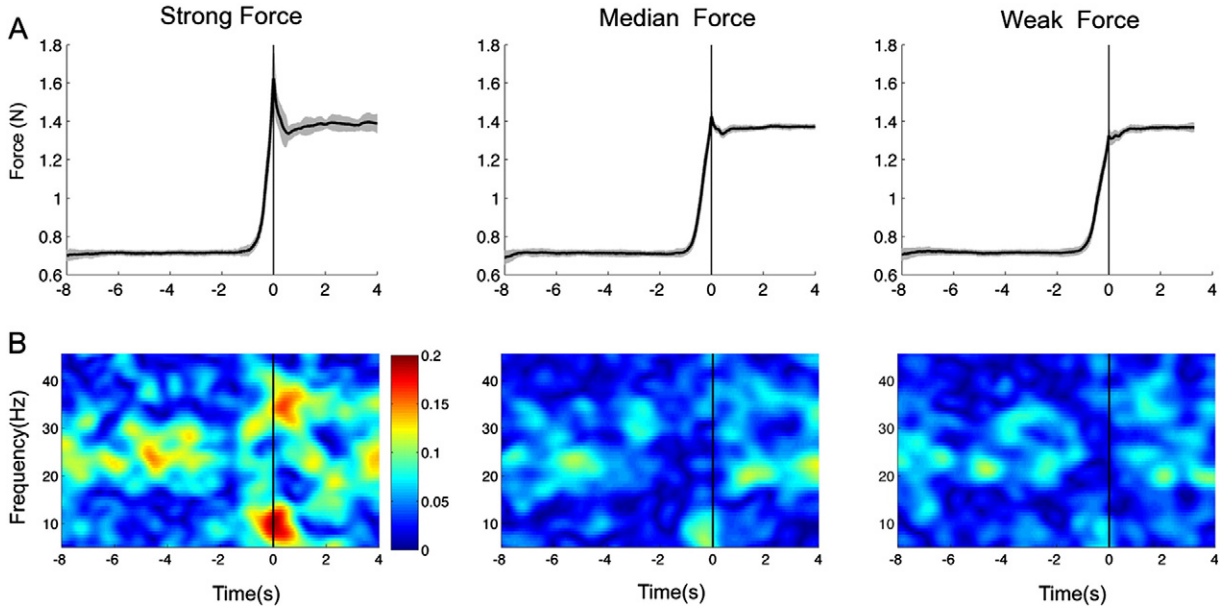

Fig. 4. Corticomuscular coherence in the three trial subgroups. (A) Average force profiles within each subgroup across 12 participants. (B) Average corticomuscular coherence spectra. Trials are sorted based on the maximum force at the end of the transition to the second target and subdivided into three subgroups of 26 trials each: maximum, medium and weak force.

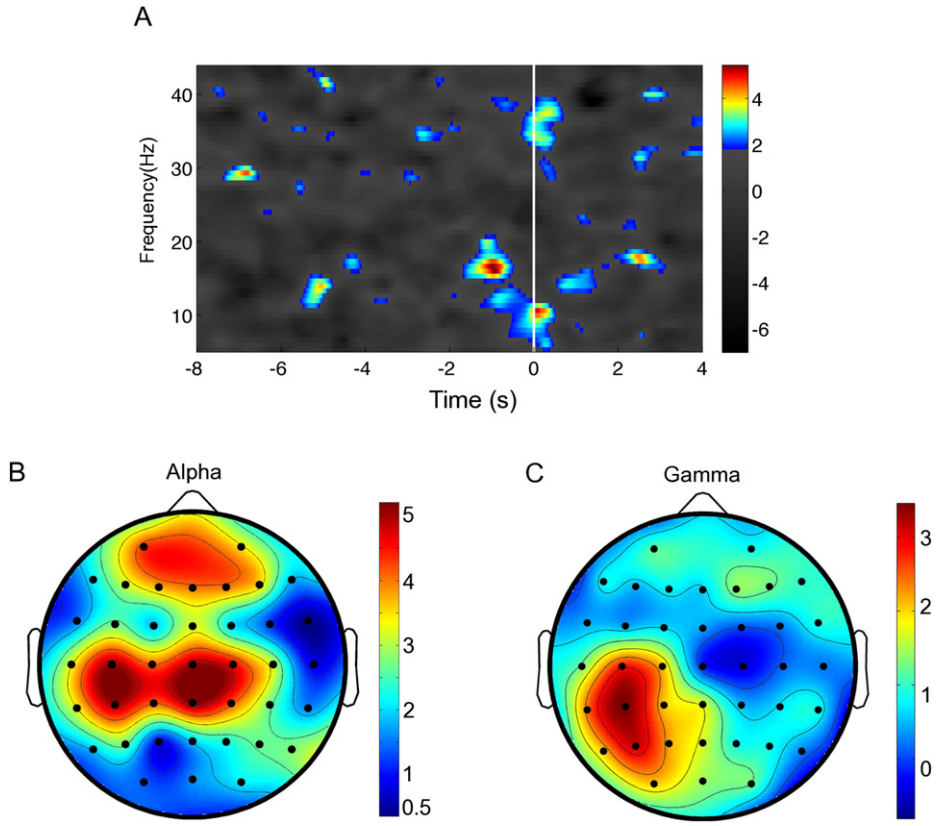

Fig. 5. Difference in corticomuscular coherence between subgroup 1 and subgroup 3. (A) T-value of the delta z-score of subgroup 1 versus subgroup 3 trials as a function of time and frequency. Significant differences in coherence ($p < 0.05$, FWE corrected) are represented in color. (B) The corresponding spatial topology of the t-value of corticomuscular coherence in the alpha band (9 Hz at $t = 0$.) (C) Spatial topology of the t-value of corticomuscular coherence in the gamma band (37.5 Hz at $t = 0$).

showed a positive time lag and in-phase coupling (reflected by the phase offset of ~2π) between EEG and EMG, and a single maximum taken place in the contralateral sensorimotor cortex. By contrast, alpha-band coherence revealed a negative time lag, anti-phase coupling (phase offset of ~π) and a more diffuse spatial topology with multiple maxima. These findings show a reorganization of corticomuscular interactions during a transition in sensorimotor state. The differences in phase offset and time lag of alpha- and gamma-band coherence suggest distinct mechanisms underlying these frequency regimes.

This is the first study to show significant corticomuscular coherence in the alpha and gamma bands during a transition between two force targets. Previous studies that used a similar experimental paradigm generally failed to show significant coherence during the transition between force levels (Baker et al., 1997; Kilner et al., 2000; Witham et al., 2011). However, these studies used a slightly different task design, where participants had to slowly change their force output from target 1 to target 2 during a 2 s interval. By contrast, in the present study participants were instructed to move from target 1 to target 2 as quickly as possible. By dividing the trials into three subgroups, we showed that corticomuscular coherence was chiefly confined to trials with the fastest transition between targets. This could explain why coherence was not observed in previous studies using a slow transition between force levels. Trials with the fastest transitions were associated with an overshoot and subsequent correction of force output. This overshoot did not occur in trials with a slow transition between force levels, which indicates that corticomuscular coherence in the alpha and gamma bands may be related to making fast movements or correcting for the associated overshoot.

We argue that corticomuscular coherence in the alpha and gamma bands observed in the present study reflects motor processing. The experimental design involves an integrated sensorimotor task in which the right index finger both generates the force and receives the vibrotactile stimuli: Alpha- and gamma-band coherence may thus result from perceptual processing of the vibrotactile stimuli, or from motor control processes involved in the transition between the two force targets. Indeed, the trials in subgroup 1 revealed faster reaction times (duration between stimulus onset and movement onset) as well as faster response times (duration between movement onset and movement endpoint), which suggests that subjects may have been more alert and attentive in these trials. Attention to tactile stimuli applied to the index finger is known to increase gamma-band activity in the somatosensory cortex (Bauer et al., 2006) and may have also contributed to the present increase in gamma-band coherence. However, Bauer and colleagues observed an increase in gamma-band activity during tactile stimulation (Bauer et al., 2006). By contrast, in the present study, there was no temporal overlap between significant alpha- and gamma-band coherence and the vibrotactile stimuli. On average, vibrotactile stimuli were presented for about 4 s before subjects initiated a response; during this interval there was no significant coherence in the alpha and gamma bands. The vibrotactile stimuli immediately ceased upon movement onset and alpha- and gamma-band coherence occurred after the onset of movement when no stimulus was presented. Brain oscillations due to sensory stimuli can last hundreds of milliseconds and are variable on trial basis, so in principle it is possible that corticomuscular coherence in both frequency bands was affected by vibrotactile stimulation. Although we found no significant effects of stimulus frequency on corticomuscular coherence (see Supplementary material), the potential influence of vibrotactile stimulation on corticomuscular coherence cannot be fully ruled out. However, if corticomuscular coherence in both frequency bands was induced by vibrotactile stimulation, one would also expect alpha- and gamma-band coherence in the trials in which no movement overshoot was made, as the same vibrotactile stimuli were delivered in those trials.

This was not the case. Hence, the most parsimonious explanation is that alpha- and gamma-band coherence was related to motor processing. Future studies using stimuli in other perceptual modalities with gradually increasing magnitude would allow further disentangling the efferent and afferent contributions to the observed corticomuscular coherence patterns.

Both the spatial topology and the phase spectra differed when comparing the corticomuscular coherence in the alpha and gamma bands. The time lag, estimated by the slope of phase difference across significant frequencies, between EEG and EMG on the frequency interval of 34–40 Hz (gamma band) was 11 ms. This was identical to the time lag that was found in the beta band during static force output. An 11-ms time lag for the beta band is consistent with previous findings, e.g., 15.9 ms (Mima et al., 2000), 9.3 ms (Gerloff et al., 2006) and 7.9 ms (Witham et al., 2011). Similarly, Schoffelen et al. (2005) found a positive slope for corticomuscular gamma-band coherence corresponding to a time delay of 7.0 ms. These results suggest that cortical activity leads muscle activity in the beta and gamma bands is consistent with the interpretation that corticomuscular beta-band coherence is primarily driven by efferent or descending pathways, although afferent or ascending pathways have shown to play a role as well (Riddle and Baker, 2005; Witham et al., 2011). By contrast, the phase spectra in the alpha band revealed a 5-ms time lag in the reverse direction, suggesting that cortical activity was here lagging EMG activity. These findings suggest that during the transition efferent processes primarily drove gamma-band coherence, whereas alpha-band coherence was dominated by afferent activity. This distinction between alpha and gamma synchronization was further supported by the phase offset and the spatial topologies: Both beta and gamma-band coherence showed in-phase coupling and a single-peaked distribution at the contralateral motor cortex. By contrast, alpha-band coherence revealed anti-phase coupling and a distinct topology at the midline frontal region. Together these results indicate that the mechanisms that govern corticomuscular coherence in the alpha and gamma bands are most likely disparate.

The phase relationship between EEG and EMG is also thought to reflect the type of interaction, in that excitatory coupling would yield in-phase coupling whereas inhibitory coupling leads to anti-phase coupling (Brillinger, 1981). Neuronal groups reveal synchronous ensemble oscillations that reflect rhythmic fluctuations in neuronal excitability and firing rate (Wang, 2010). If the coupling between sender and receiver is excitatory, increased firing rate during the 'up' state of the sender will induce rhythmic facilitation in the receiver, resulting in coinciding 'up' states or in-phase coupling. In contrast, if the coupling is inhibitory, the 'up' states of the sender will induce rhythmic inhibition and hence coincide with the 'down' states in the receiver (Fig. 6). This would imply that corticomuscular coherence in the beta and gamma bands reflects excitatory interactions while coherence in the alpha band was generated through inhibitory interactions between motor cortex and the muscle. Such an interpretation may be too simplistic as other phase relationships can be observed with asymmetric coupling and time delays (Gollo et al., 2013; Zeitler et al., 2009). However, the phase relationship may be important for the effectiveness of neuronal interactions. It has been proposed that only neuronal groups that coherently oscillate in-phase can interact effectively, because their 'windows' for communication are open at the same time (Fig. 6). The 'communication through coherence' hypothesis (Fries, 2005, 2009) suggests that selective communication is achieved through coherence between firing rate oscillation in the sending region and oscillatory gain modulation in the receiving region, which allows a network to respond selectively to task-relevant target signals while ignoring irrelevant inputs. Computational modeling demonstrates that selective communication can indeed be achieved by coherent oscillatory gain modulation, but that the structure of oscillatory activity must satisfy certain constraints (Akam and Kullmann, 2012). In particular, the target input must be differentiated from distractors by the amplitude, phase or frequency of its oscillatory modulation to avoid interference between signals. The opposite phase relationship in the alpha and gamma bands may hence allow robust dual routing of population-coded information in ascending and descending pathways.

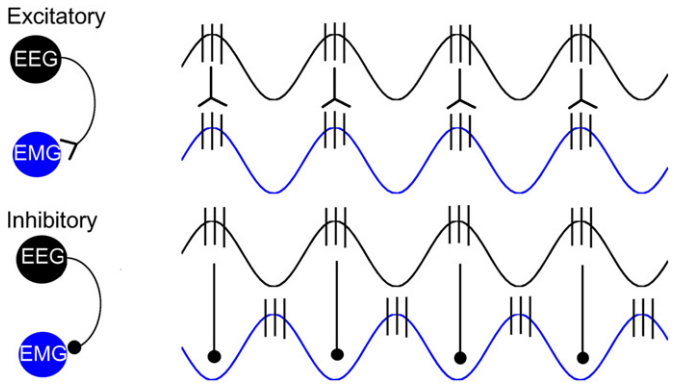

Fig. 6. Diagram of excitatory and inhibitory interactions between EEG and EMG. Top panel shows excitatory corticospinal projections resulting in in-phase coupling between EEG and EMG and the lower panel shows inhibitory projections yielding anti-phase coupling. Oscillatory activity in a group of neurons reflects rhythmic changes in excitability and affects firing rate modulation in a sending region and gain modulation in a receiving region. Adapted from Fries (2005,2009).

Similar dual-band synchrony in the alpha and gamma bands has also been observed in the visual cortex. Buffalo et al. (2011) showed a laminar difference in alpha- and gamma-band coherence in visual areas: spike-field coherence in the gamma band was largely confined to the superficial layers, whereas the deep layers showed maximal coherence in the alpha band. Their interpretation was that gamma-band coherence reflects feedforward processing, whereas alpha-band coherence most likely has a feedback function. The feedback (or top-down) function of alpha-band synchrony is supported by the time lag observed between alpha-band oscillations in the primary visual cortex and those in the association cortex, implying that the association area drives oscillations in the primary visual cortex through feedback connections (Von Stein et al., 2000). Indeed, an accumulating body of evidence emphasizes a direct involvement of alpha-band oscillations in mechanisms of top-down modulation (Jensen and Mazaheri, 2010; Palva and Palva, 2007, 2011).

Here we show a similar mechanism in the motor system, where gamma-band coherence reveals delayed EMG activity indicative of descending or feedforward interactions and alpha-band coherence showed advanced EMG reflecting ascending or feedback interactions. Alpha- and gamma-band coherence was only observed in trials in which participants made an overshoot when approaching the second target, suggesting a functional role of dual-band synchrony in error correction. Note, however, that corticomuscular coherence was maximal at 9 Hz and hence differs from typical alpha activity but may be related to the 'mu' rhythm (Pfurtscheller and Lopes Da Silva, 1999). Current motor control theories suggest that an internal model is used in trajectory planning to predict the sensory consequences of motor commands, which is updated through sensory prediction errors (Adams et al., 2013; Friston, 2010; Kawato, 1999; Shadmehr et al., 2010; Wolpert and Ghahramani, 2000). Error correction and adaption is then only required when there is a mismatch between the observed sensory signals and those predicted by the model. The observed alpha- and gamma-band coherence might hence be linked to sensory prediction errors, which would explain why this dual-band synchrony was only observed during movement overshoot. In this framework, dual-band synchrony could reflect the bilateral role of prediction errors joining sensory and motor processing (Friston et al., 2010).

Conclusions

We report multi-band synchronization in the motor system by investigating corticomuscular coherence during rapid transitions

between force targets. Corticomuscular coherence in distinct frequency bands provides different modes of neural communication between the motor cortex and spine and the reorganization of neural synchronization signifies a transition between different types of neural processing (Igarashi et al., 2013). While beta-band coherence may reflect the maintenance of the status quo, alpha- and gamma-band coherence seem to expose the feedback and feedforward interactions involved in registering a prediction error associated with movement overshoot.

Appendix A. Supplementary data

Supplementary data to this article can be found online at http://dx.doi.org/10.1016/j.neuroimage.2014.06.050.

References

Adams, R., Shipp, S., Friston, K., 2013. Predictions not commands: active inference in the motor system. Brain Struct. Funct. 218, 611–643.

Akam, T., Kullmann, D., 2012. Efficient "communication through coherence" requires oscillations structured to minimize interference between signals. PLoS Comput. Biol. 8 (11).

Amjad, A., Halliday, D., Rosenberg, J., Conway, B., 1997. An extended difference of coherence test for comparing and combining several independent coherence estimates: theory and application to the study of motor units and physiological tremor. J. Neurosci. Methods 73, 69–79.

Baker, S., 2007. Oscillatory interactions between sensorimotor cortex and the periphery. Curr. Opin. Neurobiol. 17, 649–655.

Baker, S., Olivier, E., Lemon, R., 1997. Coherent oscillations in monkey motor cortex and hand muscle EMG show task-dependent modulation. J. Physiol. 501, 225–241.

Baker, S., Kilner, J., Pinches, E., Lemon, R., 1999. The role of synchrony and oscillations in the motor output. Exp. Brain Res. 128, 109–117.

Baker, S., Pinches, E., Lemon, R., 2003. Synchronization in monkey motor cortex during a precision grip task. II. Effect of oscillatory activity on corticospinal output. J. Neurophysiol. 89, 1941–1953.

Bauer, M., Oostenveld, R., Peeters, M., Fries, P., 2006. Tactile spatial attention enhances gamma-band activity in somatosensory cortex and reduces low-frequency activity in parieto-occipital areas. J. Neurosci. 26, 490–501.

Boonstra, T.W., Breakspear, M., 2012. Neural mechanisms of intermuscular coherence: implications for the rectification of surface electromyography. J. Neurophysiol. 107, 796–807.

Brillinger, D., 1981. Time Series: Data Analysis and Theory. SIAM.

Buffalo, E., Fries, P., Landman, R., Buschman, T., Desimone, R., 2011. Laminar differences in gamma and alpha coherence in the ventral stream. Proc. Natl. Acad. Sci. U. S. A. 108, 11262–11267.

Buzsaki, G., Draguhn, A., 2004. Neuronal oscillations in cortical networks. Science 304, 1926–1929.

Cardoso, J.F., 1997. Infomax and maximum likelihood for blind source separation. IEEE Signal Process. Lett. 4, 112–114.

Cheyne, D., Bells, S., Ferrari, P., Gaetz, W., Bostan, A., 2008. Self-paced movements induce high-frequency gamma oscillations in primary motor cortex. NeuroImage 42, 332–342.

Conway, B., Halliday, D., Farmer, S., Shahani, U., Maas, P., Weir, A., Rosenberg, J., 1995. Synchronization between motor cortex and spinal motoneuronal pool during the performance of a maintained motor task in man. J. Physiol. 489, 917–924.

Engel, A., Fries, P., 2010. Beta-band oscillations—signalling the status quo? Curr. Opin. Neurobiol. 20, 156–165.

Engel, A., Fries, P., Singer, W., 2001. Dynamic predictions: oscillations and synchrony in top-down processing. Nat. Rev. Neurosci. 2, 704–716.

Farina, D., Negro, F., Jiang, N., 2013. Identification of common synaptic inputs to motor neurons from the rectified electromyogram. J. Physiol. 591, 2403–2418.

Fetz, E., 2013. Volitional control of cortical oscillations and synchrony. Neuron 77, 216–218.

Fries, P., 2005. A mechanism for cognitive dynamics: neuronal communication through neuronal coherence. Trends Cogn. Sci. 9, 474–480.

Fries, P., 2009. Neuronal gamma-band synchronization as a fundamental process in cortical computation. Annu. Rev. Neurosci. 32, 209–224.

Friston, K., 2010. The free-energy principle: a unified brain theory? Nat. Rev. Neurosci. 11, 127–138.

Friston, K., Holmes, A., Poline, J.B., Grasby, P., Williams, S., Frackowiak, R., Turner, R., 1995. Analysis of fMRI time-series revisited. NeuroImage 2, 45–53.

Friston, K., Daunizeau, J., Kilner, J., Kiebel, S., 2010. Action and behavior: a free-energy formulation. Biol. Cybern. 102, 227–260.

Gerloff, C., Braun, C., Staudt, M., Hegner, Y., Dichgans, J., Krägeloh-Mann, I., 2006. Coherent corticomuscular oscillations originate from primary motor cortex: evidence from patients with early brain lesions. Hum. Brain Mapp. 27, 789–798.

Gilbertson, T., Lalo, E., Doyle, L., Di Lazzaro, V., Cioni, B., Brown, P., 2005. Existing motor state is favored at the expense of new movement during 13–35 Hz oscillatory synchrony in the human corticospinal system. J. Neurosci. 25, 7771–7779.

Gollo, L.L., Mirasso, C., Sporns, O., Breakspear, M., 2013. Mechanisms of zero-lag synchronization in cortical motifs PLoS Comp. Biol. 10, e1003548.

Gross, J., Tass, P.A., Salenius, S., Hari, R., Freund, H.J., Schnitzler, A., 2000. Cortico-muscular synchronization during isometric muscle contraction in humans as revealed by magnetoencephalography. J. Physiol. Lond. 527, 623–631.

Gross, J., Timmermann, L., Kujala, J., Dirks, M., Schmitz, F., Salmelin, R., Schnitzler, A., 2002. The neural basis of intermittent motor control in humans. Proc. Natl. Acad. Sci. U. S. A. 99, 2299–2302.

Halliday, D., Rosenberg, J., Amjad, A., Breeze, P., Conway, B., Farmer, S., 1995. A framework for the analysis of mixed time series/point process data — theory and application to the study of physiological tremor, single motor unit discharges and electromyograms. Prog. Biophys. Mol. Biol. 64, 237–278.

Halliday, D., Conway, B., Farmer, S., Rosenberg, J., 1998. Using electroencephalography to study functional coupling between cortical activity and electromyograms during voluntary contractions in humans. Neurosci. Lett. 241, 5–8.

Igarashi, J., Isomura, Y., Arai, K., Harukuni, R., Fukai, T., 2013. A θ–γ oscillation code for neuronal coordination during motor behavior. J. Neurosci. 33.47, 18515–18530.

Jensen, O., Mazaheri, A., 2010. Shaping functional architecture by oscillatory alpha activity: gating by inhibition. Front. Hum. Neurosci. 4, 186.

Kants, H., Schreiber, T., 2003. Nonlinear Time Series Analysis. Cambridge University Press, pp. 109–112.

Kawato, M., 1999. Internal models for motor control and trajectory planning. Curr. Opin. Neurobiol. 9, 718–727.

Kilner, J., Baker, S., Salenius, S., Hari, R., Lemon, R., 2000. Human cortical muscle coherence is directly related to specific motor parameters. J. Neurosci. 20, 8838–8845.

Kristeva, R., Patino, L., Omlor, W., 2007. Beta-range cortical motor spectral power and corticomuscular coherence as a mechanism for effective corticospinal interaction during steady-state motor output. NeuroImage 36, 785–792.

Kristeva-Feige, R., Fritsch, C., Timmer, J., Lücking, C.H., 2002. Effects of attention and precision of exerted force on beta range EEG–EMG synchronization during a maintained motor contraction task. Clin. Neurophysiol. 113, 124–131.

Marsden, J., Werhahn, K., Ashby, P., Rothwell, J., Noachtar, S., Brown, P., 2000. Organization of cortical activities related to movement in humans. J. Neurosci. 20, 2307–2314.

Mehrkanoon, S., Breakspear, M., Daffertshofer, A., Boonstra, T.W., 2013. Non-identical smoothing operators for estimating time–frequency interdependence in electrophysiological recordings. EURASIP J. Adv. Signal Process. 2013, 73.

Mima, T., Steger, J., Schulman, A., Gerloff, C., Hallett, M., 2000. Electroencephalographic measurement of motor cortex control of muscle activity in humans. Clin. Neurophysiol. 111, 326–337.

Murthy, V., Fetz, E., 1992. Coherent 25- to 35-Hz oscillations in the sensorimotor cortex of awake behaving monkeys. Proc. Natl. Acad. Sci. U. S. A. 89, 5670–5674.

Omlor, W., Patino, L., Hepp-Reymond, M.C., Kristeva, R., 2007. Gamma-range corticomuscular coherence during dynamic force output. NeuroImage 34, 1191–1198.

Palva, S., Palva, J., 2007. New vistas for α-frequency band oscillations. Trends Neurosci. 30, 150–158.

Palva, S., Palva, J., 2011. Functional roles of alpha-band phase synchronization in local and large-scale cortical networks. Front. Psychol. 2, 204.

Pfurtscheller, G., Lopes Da Silva, F., 1999. Event-related EEG/MEG synchronization and desynchronization: basic principles. Clin. Neurophysiol. 110, 1842–1857.

Poline, J.B., Worsley, K., Evans, A., Friston, K., 1997. Combining spatial extent and peak intensity to test for activations in functional imaging. NeuroImage 5, 83–96.

Raethjen, J., Lindemann, M., Dümpelmann, M., Wenzelburger, R., Stolze, H., Pfister, G., Elger, C., Timmer, J., Deuschl, G., 2002. Corticomuscular coherence in the 6–15 Hz band: is the cortex involved in the generation of physiologic tremor? Exp. Brain Res. 142, 32–40.

Riddle, C., Baker, S., 2005. Manipulation of peripheral neural feedback loops alters human corticomuscular coherence. J. Physiol. 566, 625–639.

Riddle, C., Baker, S., 2006. Digit displacement, not object compliance, underlies task dependent modulations in human corticomuscular coherence. NeuroImage 33, 618–627.

Sanes, J., Donoghue, J., 1993. Oscillations in local field potentials of the primate motor cortex during voluntary movement. Proc. Natl. Acad. Sci. U. S. A. 90, 4470–4474.

Schnitzler, A., Gross, J., 2005. Normal and pathological oscillatory communication in the brain. Nat. Rev. Neurosci. 6, 285–296.

Schoffelen, J.M., Oostenveld, R., Fries, P., 2005. Neuronal coherence as a mechanism of effective corticospinal interaction. Science 308, 111–113.

Schoffelen, J.M., Poort, J., Oostenveld, R., Fries, P., 2011. Selective movement preparation is subserved by selective increases in corticomuscular gamma-band coherence. J. Neurosci. 31, 6750–6758.

Shadmehr, R., Smith, M., Krakauer, J., 2010. Error correction, sensory prediction, and adaptation in motor control. Annu. Rev. Neurosci. 33, 89–108.

Siegmund, D., Worsley, K., 1995. Testing for a signal with unknown location and scale in a stationary Gaussian random field. Ann. Stat. 23, 608–639.

Stam, C., Nolte, G., Daffertshofer, A., 2007. Phase lag index: assessment of functional connectivity from multi channel EEG and MEG with diminished bias from common sources. Hum. Brain Mapp. 28, 1178–1193.

Van Wijk, B., Beek, P., Daffertshofer, A., 2012. Neural synchrony within the motor system: what have we learned so far? Front. Hum. Neurosci. 6, 1–15.

Von Stein, A., Chiang, C., König, P., 2000. Top-down processing mediated by interareal synchronization. Proc. Natl. Acad. Sci. U. S. A. 97, 14748–14753.

Wang, X.J., 2010. Neurophysiological and computational principles of cortical rhythms in cognition. Physiol. Rev. 90, 1195–1268.

Ward, N., Farmer, S., Berthouze, L., Halliday, D., 2013. Rectification of EMG in low force contractions improves detection of motor unit coherence in the beta-frequency band. J. Neurophysiol. 110, 1744–1750.

Williams, E., Baker, S., 2009. Renshaw cell recurrent inhibition improves physiological tremor by reducing corticomuscular coupling at 10 Hz. J. Neurosci. 29, 6616–6624.

Williams, E., Soteropoulos, D., Baker, S., 2009. Coherence between motor cortical activity and peripheral discontinuities during slow finger movements. J. Neurophysiol. 102, 1296–1309.
Williams, E., Soteropoulos, D., Baker, S., 2010. Spinal interneuron circuits reduce approximately 10-Hz movement discontinuities by phase cancellation. Proc. Natl. Acad. Sci. U. S. A. 107, 11098–11103.
Witham, C., Riddle, C., Baker, M., Baker, S., 2011. Contributions of descending and ascending pathways to corticomuscular coherence in humans. J. Physiol. 589, 3789–3800.
Witte, M., Patino, L., Andrykiewicz, A., Hepp-Reymond, M.C., Kristeva, R., 2007. Modulation of human corticomuscular beta-range coherence with low-level static forces. Eur. J. Neurosci. 26, 3564–3570.
Wolpert, D., Ghahramani, Z., 2000. Computational principles of movement neuroscience. Nat. Neurosci. 3, 1212–1217.
Worsley, K., 2001. Testing for signals with unknown location and scale in a χ^2 random field, with an application to fMRI. Adv. Appl. Probab. 33, 773–793.
Worsley, K., Friston, K., 1995. Analysis of fMRI time-series revisited — again. NeuroImage 2, 173–181.
Worsley, K., Evans, A., Marrett, S., Neelin, P., 1992. A three-dimensional statistical analysis for CBF activation studies in human brain. J. Cereb. Blood Flow Metab. 12, 900–918.
Zeitler, M., Daffertshofer, A., Gielen, C., 2009. Asymmetry in pulse-coupled oscillators with delay. Phys. Rev. E Stat. Nonlinear Soft Matter Phys. 79.